Water Resources Research

RESEARCH ARTICLE
10.1029/2019WR026221

Numerical Modeling of Instream Wood Transport, Deposition, and Accumulation in Braided Morphologies Under Unsteady Conditions: Sensitivity and High-Resolution Quantitative Model Validation

V. Ruiz-Villanueva[1,2], C. Gamberini[3], E. Bladé[4], M. Stoffel[2,5,6], and W. Bertoldi[3]

[1]Institute of Earth Surface Dynamics (IDYST), University of Lausanne, Lausanne, Switzerland, [2]Climate Change Impacts and Risks in the Anthropocene (C-CIA), Institute for Environmental Sciences, University of Geneva, Geneva, Switzerland, [3]Department of Civil, Environmental and Mechanical Engineering, University of Trento, Trento, Italy, [4]Flumen Research Institute, Universitat Politècnica de Catalunya, Barcelona, Spain, [5]Department of Earth Sciences, University of Geneva, Geneva, Switzerland, [6]Department F.-A. Forel for Environmental and Aquatic Sciences, University of Geneva, Geneva, Switzerland

Abstract Large wood promotes fundamental changes in river hydraulics and morphology, playing a relevant role in river ecology but also in flood hazard. Accurate predictions of large wood dynamics in terms of deposition patterns and travel distance are still lacking and only recently have numerical models been developed to this end. In this work we enhance the capabilities of the numerical model Iber-Wood in reproducing large wood dynamics in shallow braided rivers and validate it by comparing simulations with the results of previous laboratory experiments. The flume experiments provide high-resolution observations of wood travel distances and depositional patterns of wood. The comparison proves useful to improve the numerical simulation of (i) the interactions between wood pieces and the riverbed (e.g., when wood pieces are transported by dragging), (ii) wood pieces with roots, and (iii) the formation of wood jams (i.e., accumulations of greater than three wood pieces). A sensitivity analysis reveals the crucial role of bed topography, with limited effect played by drag and restitution coefficients. Taking advantage of a controlled environment with similar simplifying hypotheses, we combine the strengths of both physical and numerical modeling to explore the parameters that are most effective in controlling wood dynamics. We use the numerical model to explore the effect of unsteady flow conditions, with different wood supply input. The resulting wood depositional patterns, jam formation, and travel distances during floods may improve our understanding of some of the controls on biogeomorphic evolutionary trajectories of braided rivers.

Key Points:
- The enhanced version of the model Iber-Wood better reproduces dragging wood transport of pieces with and without roots
- Detailed numerical simulation of the flow field allowed for the evaluation of location of wood deposition, and how the latter changes with discharge
- Numerical simulation of unsteady flow conditions showed different wood dynamics during the rising and falling limbs of floods

Supporting Information:
- Supporting Information S1

Correspondence to:
V. Ruiz-Villanueva,
virginia.ruiz-villanueva@unil.ch

Citation:
Ruiz-Villanueva, V., Gamberini, C., Bladé, E., Stoffel, M., & Bertoldi, W. (2020). Numerical modeling of instream wood transport, deposition, and accumulation in braided morphologies under unsteady conditions: Sensitivity and high-resolution quantitative model validation. *Water Resources Research*, *56*, e2019WR026221. https://doi.org/10.1029/2019WR026221

Received 23 AUG 2019
Accepted 28 MAY 2020
Accepted article online 31 MAY 2020

1. Introduction

Instream wood is nowadays recognized as one of the crucial drivers of fluvial morphology and ecology (Gurnell, 2013; Le Lay et al., 2013; Ruiz-Villanueva, Piegay, et al, 2016; Wohl, 2013, 2017; Wohl et al., 2019). However, a complete understanding of instream wood dynamics (specially in terms of transport and deposition) is still lacking. Field observations are limited, with low numbers of monitored sites, short duration of data series, and few river and forest types (e.g., Iroumé et al., 2018). Scarcity of data is exacerbated by the large spatial and temporal variability of wood availability and transport processes. Wood depositional patterns and mobility are largely affected by localized wood input from bank erosion and slopes, as well as by flood history. This makes it difficult to derive general relationships between flow parameters and wood dynamics, and to predict instream wood loads. Physical and numerical modeling may help in overcoming this limitation, as they provide exploratory tools that have proven to be fundamental for a better understanding of the role of different parameters, such as changes in wood properties, wood input rate, water discharge, or riverbed morphology (Bertoldi & Ruiz Villanueva, 2017; Paola et al., 2009). Physical modeling also provides high-resolution data, including details on wood entrainment, transport or deposition, which are rarely measured in the field. Probably one of the first laboratory experiments investigating instream wood dynamics was presented by Braudrick et al. (1997), where the authors analyzed wood dispersion in a mobile bed channel flume. Only very few experiments have been performed so far with mobile bed conditions. Recently,

Davidson et al. (2015) investigated wood stability and transport in "small" rivers, where wood length was assumed similar to channel width. They evaluated the time scale needed by newly recruited wood pieces to self-organize into more stable jams. Welber et al. (2013) and Bertoldi et al. (2014) investigated the deposition pattern of wood in large braided rivers, where the abundance of exposed sediment bars and the frequent bank erosion provide suitable conditions for wood recruitment and deposition. These experiments quantified the role of wood piece dimension and river morphology in driving wood deposition patterns.

The use of numerical models (i.e., computational fluid dynamic (CFD) models) to simulate wood transport started only recently. The first attempts, however, did not include wood as an additional element, but rather used the outputs from 1-D-CFD or 2-D-CFD models (i.e., water depth and flow velocity) to explain wood motion and entrainment, to predict possible wood trajectories (Mazzorana et al., 2011; Merten et al., 2010), and to test various river restoration designs (Hafs et al., 2014).

The first fully coupled wood transport CFD model was the Iber-Wood model developed by Ruiz-Villanueva, Bladé, et al. (2014). This model combines an Eulerian approach for flow and sediment with a Lagrangian (i.e., discrete element) approach for wood elements. Recently, a similar approach has been used by Persi et al. (2016) and Kang and Kimura (2018). Iber-Wood was initially tested with flume experiments in a simple straight channel (see Ruiz-Villanueva, Bladé, et al., 2014) and proved to accurately reproduce floating transport, general patterns of wood deposition, and impacts on hydrodynamics. It was later applied to several case studies (e.g., Ruiz Villanueva, Bladé Castellet et al., 2014; Ruiz-Villanueva, Piégay, Gurnell, et al., 2016; Ruiz-Villanueva et al., 2017) for which some field information was available to validate model results. In addition, the model has been used in an exploratory manner, that is, to test the existence of threshold behaviors and tipping points, or to identify the factors controlling wood transport and deposition rather than reproducing a specific flood event or predicting the movement of single wood pieces (Ruiz-Villanueva, Wyzga, Hajdukiewicz, & Stoffel, 2016). As usual, with numerical models, the initial version of Iber-Wood had several simplifications. One important simplification was the assumption that wood pieces are cylinders (i.e., logs), thereby ignoring the presence of roots. Another simplification concerned log-log interactions (i.e., wood pieces interactions), considered as elastic, and the accumulation of wood in jams, which is a fully 3-D process, and thus challenging to be fully reproduced by a 2-D model. In addition, only floating wood transport was fully validated, whereas detailed wood dragging validation was lacking. Some of these constraints resulted from the lack of observations and data with adequate resolution.

The first objective of this work therefore was to enhance the capabilities of the Iber-Wood model in order to better simulate log-log, log-banks, and log-bed interactions and to validate the changes by comparing the model results with high-resolution data from available flume experiments and current knowledge on wood dynamics in braided rivers. In addition, we carried out a sensitivity analysis to investigate the effect of different model input parameters related to these processes. To achieve this objective, we exploited the detailed data set reported in Welber et al. (2013).

With this improved version of the model, we also followed a second objective: to explore and to better understand wood deposition by analyzing the details of the flow field, considering both steady and unsteady discharge and wood supply conditions in braided systems.

2. Material and Methods

2.1. Iber-Wood

Iber-Wood is a two-dimensional numerical model that couples an Eulerian model used for hydrodynamics (i.e., Iber) to a Lagrangian or discrete element model simulating the motion of individual pieces of wood (Ruiz-Villanueva, Bodoque, et al., 2014). Iber and Iber-Wood have been presented in several publications (Bladé Castellet et al., 2014; Ruiz-Villanueva, Bodoque, et al., 2014; Ruiz Villanueva, Bladé Castellet et al., 2014; Ruiz-Villanueva et al., 2017; Ruiz-Villanueva, Wyzga, Hajdukiewicz, & Stoffel, 2016; Ruiz-Villanueva, Wyżga, Mikuś, et al., 2016; Ruiz-Villanueva, Wyzga, Zawiejska, et al., 2016); therefore, we describe here only the main aspects and the new features and improvements implemented during the course of this work in the model, referring to previous works for the general functioning.

Iber solves the hydrodynamics (the 2-D Saint Venant or Shallow Water Equations), turbulence (using several turbulence models) and sediment transport (solving the 2-D Exner equation for bed and suspended load applying different equations) by using the finite volume method with a time explicit second-order and non-oscillatory extension of Roe's upwind scheme on nonstructured meshes (Bladé Castellet et al., 2014). Wet-dry fronts, both stationary and nonstationary, are modeled with a fixed finite volume mesh, and a wet-dry tolerance. For the presented work this tolerance was decreased from a common value for rivers equal to 0.01 to 0.0005 m.

Iber-Wood fully couples wood and hydrodynamics by adding a wood drag term to the two-dimensional Saint Venant equations. The model simulates individual cylindrical pieces of wood (i.e., logs) determining their initial motion by computing the balance of forces acting on the log's center of mass. Therefore, the incipient motion calculation is fully dynamic. The main parameters involved in the governing equations are wood density, angle of the log relative to the flow, log length, log diameter, friction coefficient between the log and the riverbed, and drag coefficient of the log in water. Two transport mechanisms (i.e., floating or sliding on the riverbed) are possible according to wood buoyancy and flow conditions. If the wood piece is floating, its velocity is assumed to be the same as the flow velocity (as observed by Macvicar et al., 2009), unless turbulence is considered. Turbulent fluctuations affect wood, introducing a random component into its motion, thereby adding a partial stochastic (i.e., nondeterministic) component to the model (see Ruiz-Villanueva et al., 2017, for details). If wood buoyancy is low, and flow is shallow, as usual in braided morphologies, wood may not float but drag or slide. When the piece of wood is transported dragging, its velocity is different from the flow velocity, and the friction force is the main factor controlling the movement of wood.

Wood pieces may rotate adjusting their angle to the flow velocity field, and they may also interact between each other and/or with channel boundaries, including infrastructures (see Ruiz Villanueva, Bladé Castellet et al., 2014, Ruiz-Villanueva et al., 2017, for details). Wood-wood interactions (computed as collisions of cylindrically shaped rigid bodies) can be elastic or inelastic, a condition that is defined by the restitution coefficient (e.g., if the restitution coefficient is equal to 1 the collision is elastic). In previous works, elastic collisions were assumed by default. If a moving log collides with another log (both pieces floating, sliding/dragging, or resting), velocities and trajectories are recalculated. The recent changes made in the model code during this work improved this log-log interaction by accounting for the impact force. If one of the pieces is resting, the impact force of the second log must be larger than the friction force of the first to entrain the latter. If this condition is not satisfied the second piece is deposited and an accumulation (i.e., jam) may form. Previous versions of Iber-Wood assumed that jams formed only if wood pieces stopped due to the increase in resting forces (i.e., friction force) but without considering the effect of impact forces. Wood-bank (or log-dry area) interactions have been improved as well in the latest version of Iber-Wood presented here, and they are now simulated using two different approaches. If the bank slope is steep (the bank angle is higher than the friction angle) log movement is treated as if it would hit a wall (this was the approach used in previous versions of Iber-Wood), and the model considers that the log may slide or glide parallel to the bank (or wall) or may bounce off and change its trajectory suddenly, based on the log incidence angle threshold (45° by default). If the bank slope is smaller than the friction angle, the log can be partially deposited on a dry zone, or part of the log length could rest in shallow water. In that situation, the driving forces (acting only along the wet length of the log) decrease and the piece can be entrapped on the bank.

Iber-Wood initially considered the wood pieces as straight simple cylinders, neglecting the presence of branches and roots. Here we overcome this limitation by modifying the model to consider also wood pieces with roots, assuming roots as an attached short or flat cylinder to the log. Wood with roots are thus defined by their log length and diameter (L_w and D_w), and the diameter (i.e., root length) and thickness of the root wad (L_r and W_r). The presence of roots affects the friction, gravity and drag forces acting on the log as follows:

$$F_f = -\left(g \cdot \rho_w \cdot L_w \cdot \left(\left(\pi \cdot D_w^2\right)/4\right) + W_r \cdot \pi \cdot L_r^2\right) - \left(g \cdot \rho \cdot \left(V_1 + V_2\right)\right) \cdot \cos(\alpha)\right) \cdot F_c \quad (1)$$

$$F_g = \left(g \cdot \rho_w \cdot \left(L_w^* \left(\left(\pi \cdot D_w^2\right)/4\right) + W_r \cdot \pi \cdot L_r^2\right) - \left(g \cdot \rho \cdot \left(V_1 + V_2\right)\right) \cdot \sin(\alpha) \quad (2)$$

$$F_d = \left(\left(A_1 + A_2\right) \cdot \sin(\theta) + A_3 \cdot \cos(\theta)\right) \cdot 1/2 \cdot U^2 \cdot C_d \cdot \rho \quad (3)$$

where g is gravity, ρ and ρ_w are the water and wood densities respectively, F_c is the friction coefficient, α is the bed angle, θ is the angle of the wood piece with respect to the flow direction, C_d is the drag coefficient,

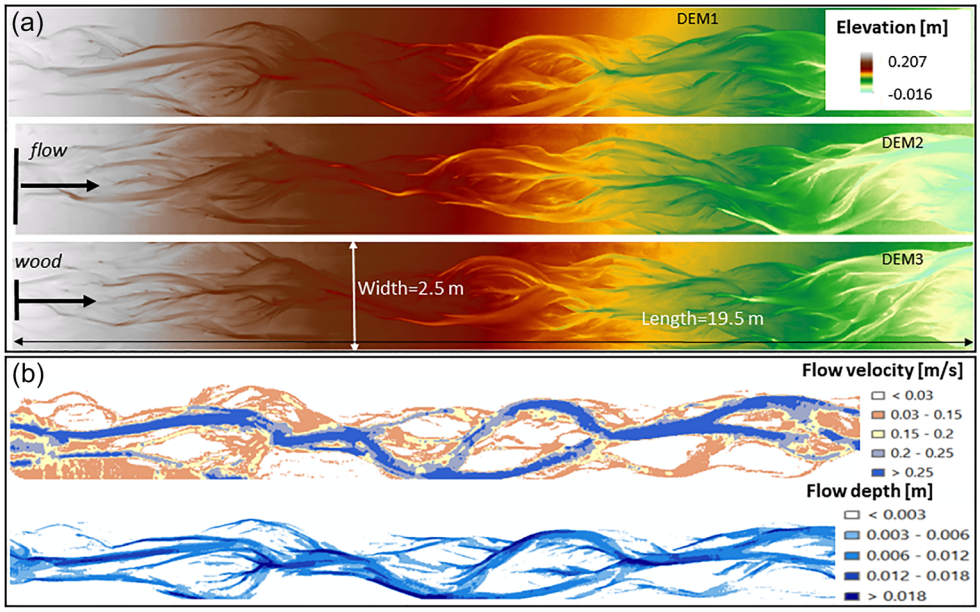

Figure 1. (a) The three digital elevation models used for the numerical modeling; (b) numerical model results for flow velocity and flow depth for DEM 1 and 1.8 l/s discharge.

V_1 and V_2 are the submerged volumes of the wood piece and rootwad, respectively, and A_1 and A_2 are the submerged areas of the wood piece and rootwad; A_3 is the submerged area of the rootwad perpendicular to piece length. This approximation only considers the frontal area of the rootwad, which has been proved the relevant parameter influencing the motion of wood with roots (Ghaffarian Roohparvar, 2014). These equations differ from those included in Iber-Wood for wood pieces without roots (see Ruiz-Villanueva, Bladé, et al. 2014, for details).

Initial tests of this capability showed that the main effect of the presence of roots is the increase in resisting forces, as roots may contact the riverbed increasing the friction, depending on the buoyancy. Furthermore, rooted pieces are more likely to rotate, with the roots pointing upstream (see Comper et al., 2018).

Iber-Wood requires initial and/or inlet boundary conditions for wood. Initial conditions are entered as the exact position of each log, its dimensions (i.e., length and diameter), density, and orientation, usually for the initial time step, or any other time step of the simulation. Wood inlet boundary conditions can be assigned to the simulation domain boundaries (one or more inlets are possible), giving a wood rate or number of wood pieces per minute as well as ranges of its characteristics (i.e., maximum and minimum lengths, diameters, and density of wood), which are used to characterize each single piece entering the simulation by means of stochastic variations. This stochastic characterization of inlet wood, together with the effect of turbulence on wood motion, result in a partial nondeterministic nature, which enables repetition of each simulation resulting in slightly different results.

2.2. Flume Experiments

The flume experiments were carried out at the Hydraulics Laboratory of the University of Trento (see Welber et al., 2013 for more details). The experiments reproduced braided morphologies in a 3 m wide, 25 m long flume, filled by a well-sorted sand with median grain sizes of 1.03 mm (Figure 1a). Runs were performed with a constant longitudinal gradient equal to 0.01 m/m and with water discharge ranging from 0.9 to 1.8 l/s. This range includes four different flow conditions between 50% and 100% of the formative discharge (i.e., 1.8 l/s; Welber et al., 2013). Flume bed topography was surveyed by a laser profiler mounted on a carriage covering a large part of the flume (2.5 m wide, 22 m long), with a resolution of 0.05 m downstream and 0.005 m along cross sections (Figure 1b). Vertical images were acquired by a digital camera mounted on a 4 m high, movable metal frame.

In-channel wood was modeled by adding cylindrical wood dowels with varying length (0.04–0.12 m), diameter (0.003–0.008 m), and proportion of logs with roots (0–100%), reproduced by the addition of cross-shaped, 12 mm wide, elements. Dowels were designed to reproduce conditions that are similar to those observed in the Tagliamento river (Bertoldi et al., 2013; Welber et al., 2013). This means that both the dowel length was chosen according to the channel width (to reproduce "large" river conditions) and the dowel diameter was defined according to water depth so as to the ensure similar floating conditions. Wood dowels were inserted in a large and deep anabranch, with a rate of 15 logs per minute to avoid congested wood transport conditions. Wood depositional patterns were mapped visually in the flume and described in terms of travel distance and accumulation size. A large number of repeated experiments were performed, so as to take the variability of the wood input location into account and to explore the role of different controlling parameters (i.e., log diameter, length, and flow discharge).

2.3. Numerical Model Calibration, Validation, and Sensitivity Analysis

The laboratory data were used to assess the performance of the enhanced model in a quantitative way, allowing for the first time a detailed and high-resolution model validation. In particular, the new features implemented in the numerical model were accurately checked, with specific attention paid to wood sliding or dragging on the bed, wood-wood interactions, and jam formation.

Three different braided morphologies obtained in the laboratory experiments were used in this study (Figure 1).

The three digital elevation models were transformed into a regular calculation mesh, with a resolution equal to 5 mm using the Geospatial Data Abstraction Library (GDAL) approach (GDAL/OGR contributors, 2019). Discharge (critical/subcritical conditions) and wood inlet boundary conditions were assigned to the upstream boundary (Figure 1), and subcritical conditions were assigned to the outlet boundary. For each DEM, the wood inlet boundary condition was assigned to several mesh elements (between 5 and 7) located at the most upstream boundary of the main channel. Changing the wood inlet boundary condition allowed us to repeat the simulation with the same setup, and to assemble the results, as was done for the flume experiments. Pieces of wood entered the domain as soon as the hydrodynamics reached the steady condition (i.e., as soon as the difference between the inlet and outlet flows is negligible) or distributed along the hydrograph (see section 2.4).

Calibration of the hydrodynamics (based on the calibration of roughness coefficient) was performed by classifying wet and dry areas in the numerical model domain and compared to wet and dry areas observed in the flume for one topography (i.e., DEM1) using the four discharges used in the flume (i.e., 0.9, 1.2, 1.5, and 1.8 l/s) and four roughness coefficients (Manning values equal to 0.013, 0.014, 0.016, and 0.018 s $m^{-1/3}$). Spatially distributed maps of water depth or flow velocity were not available from the flume experiments; therefore, orthogonal images taken in the flume during the experiments were used to map dry and wet areas. These maps were compared with results from the numerical simulations and the misclassified area (i.e., observed dry areas modeled as wet and observed wet areas modeled as dry) was computed to get an error. A Manning coefficient equal to 0.014 s $m^{-1/3}$ was selected based on the comparison with observations. With this choice, the error between observed and modeled inundation patterns ranged between 8% and 13% (mean value equal to 11%) for the four discharges simulated, and the total wet area was accurately reproduced, with a small overestimation of the numerical model.

Before reproducing the full set of flume experiments, we carried out a sensitivity analysis to test the relative effect of three user-defined numerical model input parameters (the drag and friction coefficients and the restitution coefficient) on log dynamics and deposition, quantified by the log travel distance. The drag coefficient refers to the drag on individual logs, friction refers to the friction between logs and channel boundaries and the restitution coefficient defines the log-log interactions. Ranges for these parameters are reported in Table 1, along with references to modeling studies. The simulations used for the sensitivity analysis were realized with DEM1 (see Table 2).

2.4. Numerical Modeling Setup

Following the same approach of the laboratory experiments, we defined different sets of model runs aimed at separately investigating the influence of different factors on wood mobility in braided morphologies. The first three sets reproduced the experiments realized in the laboratory and aimed at exploring the effect of

Table 1
Coefficients Tested in the Sensitivity Analysis

Coefficient	Value used in the sensitivity analysis	Values proposed in literature	Reference and comments
Drag (C_d) [-]	0.6	0.7–0.9	Shields & Gippel (1995)
	1	0.8	Mazzorana et al. (2011)
		1.2	Brooks et al. (2006) (real logs)
		0.4–1.2	Gippel et al. (1996)
	1.41	1.41	Bocchiola et al. (2006) (dowels in flume)
		1.5	Alonso (2004)
		1.34–1.45	Boothroyd et al. (2017) (for submerged vegetation)
	1.8	values up to 4	Hui et al. (2010) (for leafy shrubs)
	Variable	Variable	Gippel et al. (1996) (Cd varies according to the orientation)
Friction (F_c) [-]	0.2	0.2	Bocchiola et al. (2006)
	0.47	0.47	Ishikawa et al. (1989) (for floating logs in debris flows)
	0.62	0.62	Buxton (2010)
	1.2	1	Mazzorana et al. (2011)
	1.6		—
Restitution (R_c) [-]	0.1		—
	0.2		—
	0.6		—
	1		—

(i) wood size (Set T1), (ii) inlet discharge (Set T2), and (iii) presence of roots (Set T3). These sets allowed direct comparison with flume results and produced an accurate verification of the numerical model performance. Moreover, the numerical model allowed us to further analyze the flow field and elevation of deposited logs. In addition, two sets were designed to extend the analysis of wood dynamics in braided rivers, investigating the effect of (i) a mixture of logs with different lengths and diameters (Set T4) and (ii) different wood input rates under unsteady flow conditions (Set T5).

Wood logs dimension and input rate varied in the different sets and are described in Table 2. In all numerical runs, wood density was set to 800 kg/m^3 and we used fixed values 8 except in the sensitivity set of friction, drag, and restitution coefficients (0.47, 1.41, and 1, respectively). Three different wood supply rates were simulated in Set T5: (i) steady rate of 16 logs/min during the rising limb, (ii) steady rate of 8 logs/min during the rising limb, and (iii) unsteady wood rate as a power function of the water discharge (Figure 2), with an exponent equal to 4.5, as suggested by Turowski et al. (2013). Simulations of Set T5 used a triangular hydrograph, with a peak discharge equal to 1.8 l/s and a duration of 40 min (Figure 2).

Results were analyzed in terms of travel distance, computed as the difference between the longitudinal coordinates of the depositional site and input point, for each deposited log. Initially, for the analyses we only

Table 2
Simulation Parameters for the Different Sets of Numerical Runs

Set	Target variable	Length (L) (cm)	Diameter (D) (mm)	Roots (-)	Discharge (l/s)	DEM	Wood inlet cells (used for ensembled results)	Number of runs	Number of inlet logs[a]	Number of deposited logs[a]	Averaged deposition ratio (Dr) (%)
Sensitivity	Drag, friction and restitution coefficients	8	3	No	1.8	1	5	60	1911	1,465	77
T1	Log diameter and length	4, 6, 8, 12	2, 3, 4, 6	No	1.8	1, 2, 3	7	147	3,345	2,244	67
T2	Flow discharge	8	3	No	0.8, 1.2, 1.5, 1.8	1, 2, 3	7	84	1,436	981	68
T3	Presence of roots	8	3	Yes	1.8	1, 2, 3	7	21	480	404	84
T4	Variable wood sizes	Variable 8–12	Variable 3–6	No	1.8	1, 2, 3	7	21	478	369	77
T5	Unsteady wood supply and flow	8	3	No	Hydrograph	2	7	21	356	230	63

[a]Sum of all runs in a set.

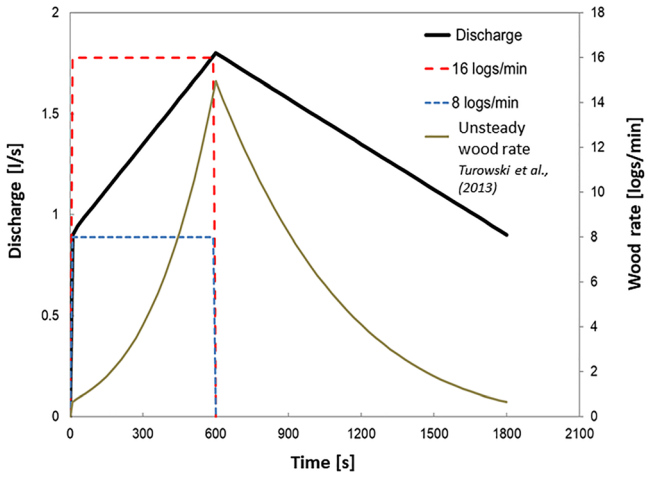

Figure 2. Hydrograph and wood supply for Set 5: (i) steady rate of 16 logs/min during the rising limb; (ii) steady rate of 8 logs/min during the rising limb; (iii) unsteady wood rate as a power function of the water discharge, with an exponent equal to 4.5, as suggested by Turowski et al. (2013).

considered logs that were deposited within the domain at the end of the simulation, without counting the logs that were transported downstream through the outlet boundary (i.e., exited logs), as it was done in the flume experiments. However, we observed that in the numerical simulations, the number of exited logs was higher than in the laboratory. On average for all runs, ~2% of the logs exited the flume in the laboratory, whereas in some numerical runs, between 20% and 30% exited the domain. Under such circumstances, we assumed that all numerically modeled exited logs traveled a distance that was at least equal to the length of the simulation domain (i.e., >20 m). This assumption implies that the data obtained in this study can be considered censored data (e.g., Helsel, 2012) as the exact travel distance is unknown. To analyze this type of data, we applied a survival analysis by computing their probability fitting the travel distance to survival curves using the Kaplan-Meier method and the significance by the log rank test (Bewick et al., 2004). We compared the numerical results containing all logs (including the exited logs) with the numerical results containing only the deposited logs, as well as with the laboratory observations.

To be able to compute different repetitions of each numerical run, similarly to what was done in the flume (experiments were repeated 10 times), we assigned the inlet boundary condition (i.e., input point) for wood to 5 (for the sensitivity analysis set) and 7 (for all other sets) boundary cells and we ensembled the results from these 5 and 7 run repetitions in terms of frequency distributions and median travel distance. Number of deposited single logs, log accumulations and the spatial patterns of wood deposits were also analyzed. Log accumulations were classified into four classes (jams formed by 2, 3, 4 to 9, and more than 9 logs) and the proportion of logs in each jam size class was computed and compared with the flume observations.

Statistical analyses were realized with the software RStudio Version 1.2.1335 (Rstudio Team, 2018). Differences within the sets (i.e., between the groups of runs) were computed by the nonparametric Wilcox (Mann-Whitney) or Kruskal-Wallis tests for two or more groups respectively (*Stats* package; R Core Team, 2019). When testing differences between more than two groups, we identified which pairs of groups were different by applying a post hoc pairwise comparison test with the Bonferroni correction for multiple testing (*Stats* package; R Core Team, 2019). The survival analysis was performed using the *survival* and *survminer* packages (Kassambara et al., 2019; Therneau, 2015; Therneau & Grambsch, 2000). Significance was set to p value <0.05. The dependence of travel distance of deposited logs on multiple controlling variables was verified by means of multiple regression analysis, with wood diameter, wood length, and discharge as independent variables.

3. Results

3.1. Model Calibration and Sensitivity Analysis of Wood Parameters

The numerical results from the sensitivity set showed that according to the survival analysis, the probability distribution of the travel distance of all logs (including logs that exited the domain) was significantly different for the different runs using the different values of the drag and friction coefficients and for the three DEMs (Figure 3). The largest variability in terms of probability of travel distance was found for the runs using the different friction coefficient values and the runs using the different DEMs. According to these results, the restitution coefficient was not very relevant in terms of travel distance probability.

Analysis of the ensembled median travel distance of all logs (i.e., deposited and exited logs) and only the deposited logs revealed more details about the differences observed in the survival analysis (Figure 4).

Figure 4 also shows the percentage of logs that exited the simulation domain at the outlet (i.e., deposition ratio, Dr). For this set of runs, Dr ranged between 53% and 88% (mean = 77%). This means that between 13% and 47% of the supplied logs exited the simulation domain.

The observed differences between the runs using different drag coefficients mostly stem from the run with a very low value (i.e., 0.6), which significantly reduced the travel distance (according to the ad hoc test). The

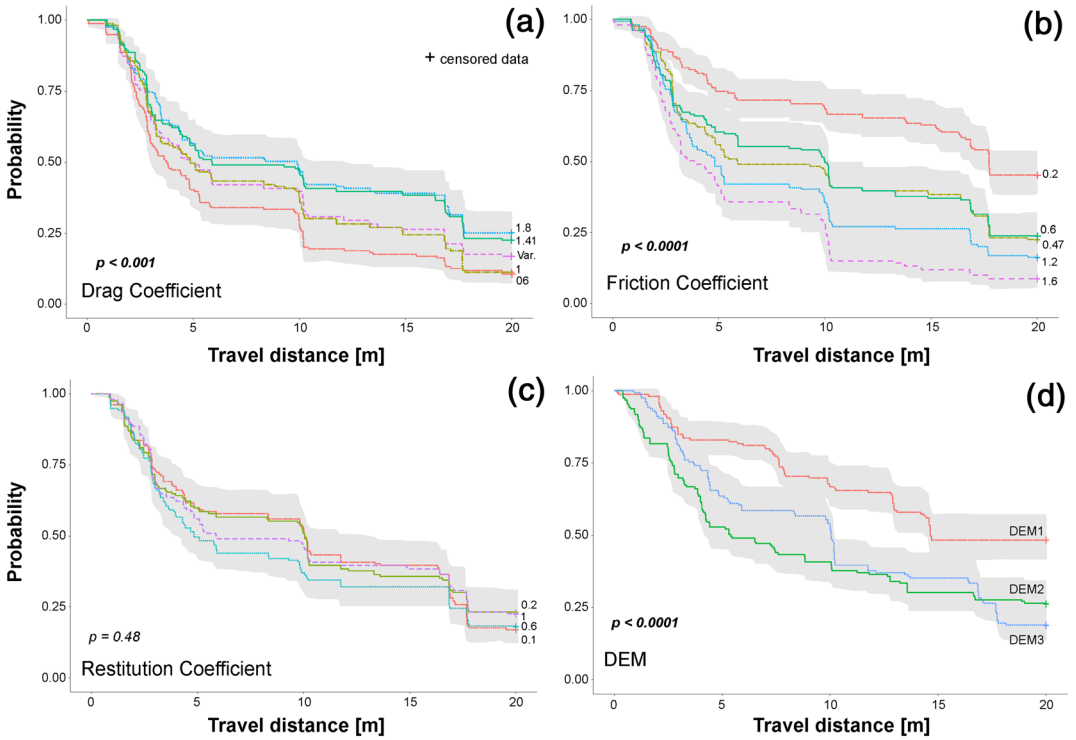

Figure 3. Survival curves (i.e., probability distribution) of travel distance by all logs for the different runs of the sensitivity set, using different values of (a) drag, C_d, (b) friction, F_c, and (c) restitution, R_c, coefficients modeled using the DEM1, and (d) for three runs using a fixed set of coefficients (i.e., $C_d = 1.41$, $F_c = 0.47$, and $R_c = 1$) and the three different DEMs. Gray areas show the confidence intervals. The p value is from the log rank test.

differences observed between the simulations with different friction coefficient were more important (i.e., the travel distance significantly varied for the different coefficient values). A very low value (0.2) of friction coefficient significantly increased the ensemble median travel distance and reduced the number of logs deposited within the simulation domain, whereas a very high value (1.6) had the opposite effect. Figure 4 finally shows that a very low value of restitution coefficient (0.1) also affected the travel distance of logs. However, such low values of drag, friction, and restitution coefficients are not reliable for cylindrical wooden logs (see Table 1); therefore, the runs of this set are not directly comparable to the flume experiments.

In addition to the sensitivity set runs, we also tested whether flume morphology had an influence on the distance traveled by logs. For these runs and the other simulated sets (T1–T5), we fixed the values for the three coefficients as follows: $C_d = 1.41$, $F_c = 0.47$, and $R_c = 1$. As Figures 3 and 4 show, we found significant differences in the travel distance of logs modeled using the three DEMs. Despite that the three DEMs were very similar at the reach scale (e.g., with a similar bed relief, hydrodynamics, number of anabranches, similar size of channels, and bars; Table 3), they were locally different, in terms of the location and sequence of exposed bars, bifurcations, and confluences. These spatial differences had a large impact on wood dynamics, as logs were exposed to different sequences of fast and deep versus slow and shallow areas.

These results revealed the important role of the friction between logs and the bed (as many logs do not just float but also slide on shallow water depths and on bars), and of the river morphology as a variable controlling wood transport and deposition in braided rivers.

3.2. Sets T1 and T2: The Role of Wood Size and Flow Conditions

As observed in the flume and in the simulations, log diameter appears to be the dominant factor governing travel distance in braided rivers. Logs with the smallest diameters traveled significantly longer distances both in the flume and in the numerical model considering all logs and only deposited logs (Figures 5a–5c). The role of log length was not significant and the pattern was more complex, with median travel distance peaked for intermediate values of length, both in flume experiments and numerical

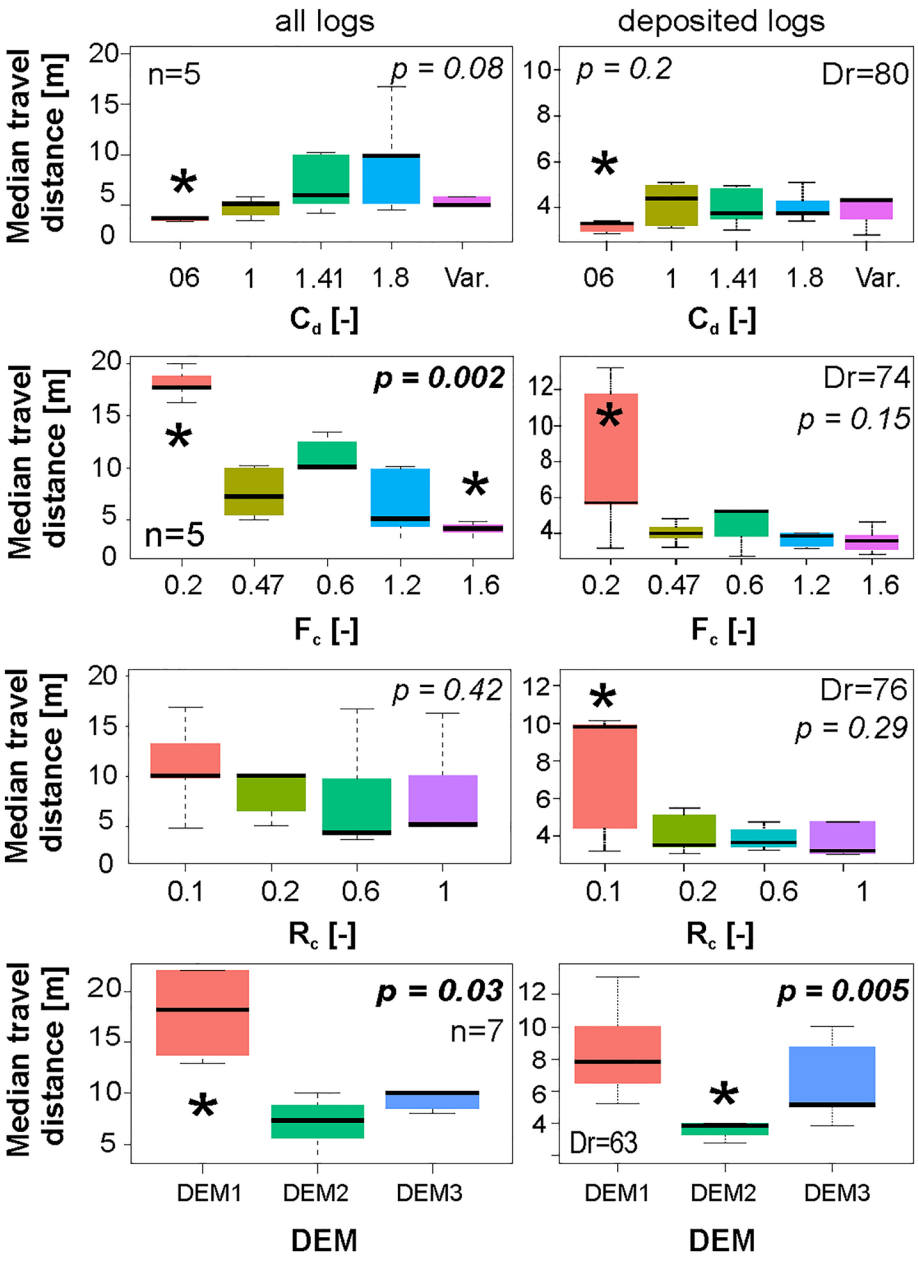

Figure 4. Boxplots of ensemble median travel distance computed for all logs (deposited and exited logs) and for deposited logs only, for different values of drag C_d, friction F_c, and restitution R_c coefficients; and runs using the three DEMs. The boxplot represents the minimum (i.e., smallest value within 1.5 times interquartile range below 25th percentile), maximum (i.e., largest value within 1.5 times interquartile range above 75th percentile), median, first quartile (i.e., 25th percentile), and third quartile (i.e., 75th percentile), outliers are not shown; Dr shows the deposition ratio as a percentage (%). The *p* values are from the Kruskal-Wallis test, the black stars show the groups that are significantly different according to the post hoc test.

simulations of deposited logs (Figures 5d–5f). Two general observations about the numerical results is that variability of travel distance between the ensembles seems to be smaller, and logs traveled over longer distances than observed in the flume, particularly when considering also the logs that exited the flume. These aspects are further analyzed in the discussion. The mean deposition ratio for numerical runs in Set 1 was equal to 67% (ranging between 42% and 97%).

As observed in the flume, the numerical model showed that logs traveled longer distances during the largest discharge (1.8 l/s), while logs traveled slightly shorter and similar distances for the other discharges (Figures 5g–5i), but differences were not significant.

Table 3
Statistics of the Three DEMs Used for the Numerical Simulations

	DEM1	DEM2	DEM3
	Detrended elevation (m)		
MIN	−0.048	−0.039	−0.041
MAX	0.022	0.025	0.035
MEAN	0.0	0.0	0.0
SDV	0.007	0.007	0.007
	Simulated water depth for $Q = 1.8$ l/s (m)		
MIN	0.0005	0.0005	0.0005
MAX	0.0411	0.0413	0.0415
MEAN	0.0058	0.0051	0.0056
SDV	0.0054	0.0049	0.0050
	Simulated flow velocity for $Q = 1.8$ l/s (m/s)		
MIN	0.0	0.0	0.0
MAX	0.4510	0.5113	0.4860
MEAN	0.1529	0.1546	0.1601
SDV	0.0917	0.0916	0.0968

We also computed a multiple linear regression model using the deposited logs data set from the numerical runs in Set T1, and the obtained model confirmed our results. The log diameter and discharge significantly explained travel distance, with negative and positive regression coefficients, respectively, and values >1 (p value < 0.005), and log length being not significant (p value 0.48). Although the variance explained by the model was only 40% ($R^2 = 0.4$).

The numerical model allowed us to further analyze log deposition. Results show that the elevation of the deposited logs did not vary significantly with discharge (Figure 6). All logs were deposited on a relatively small range of 0.01 m in bed elevation, with a majority of them being deposited on a detrended bed elevation that ranges from −0.002 to +0.003 m, corresponding to roughly one log diameter below or above average bed elevation. Although differences were not significant (see boxplots in Figure 6), overall more wood deposited at the highest elevations at higher discharges (as shown by the cumulative frequency curves in Figure 6).

The wood depositional pattern could be better explained investigating the flow field more in detail using the numerical model results.

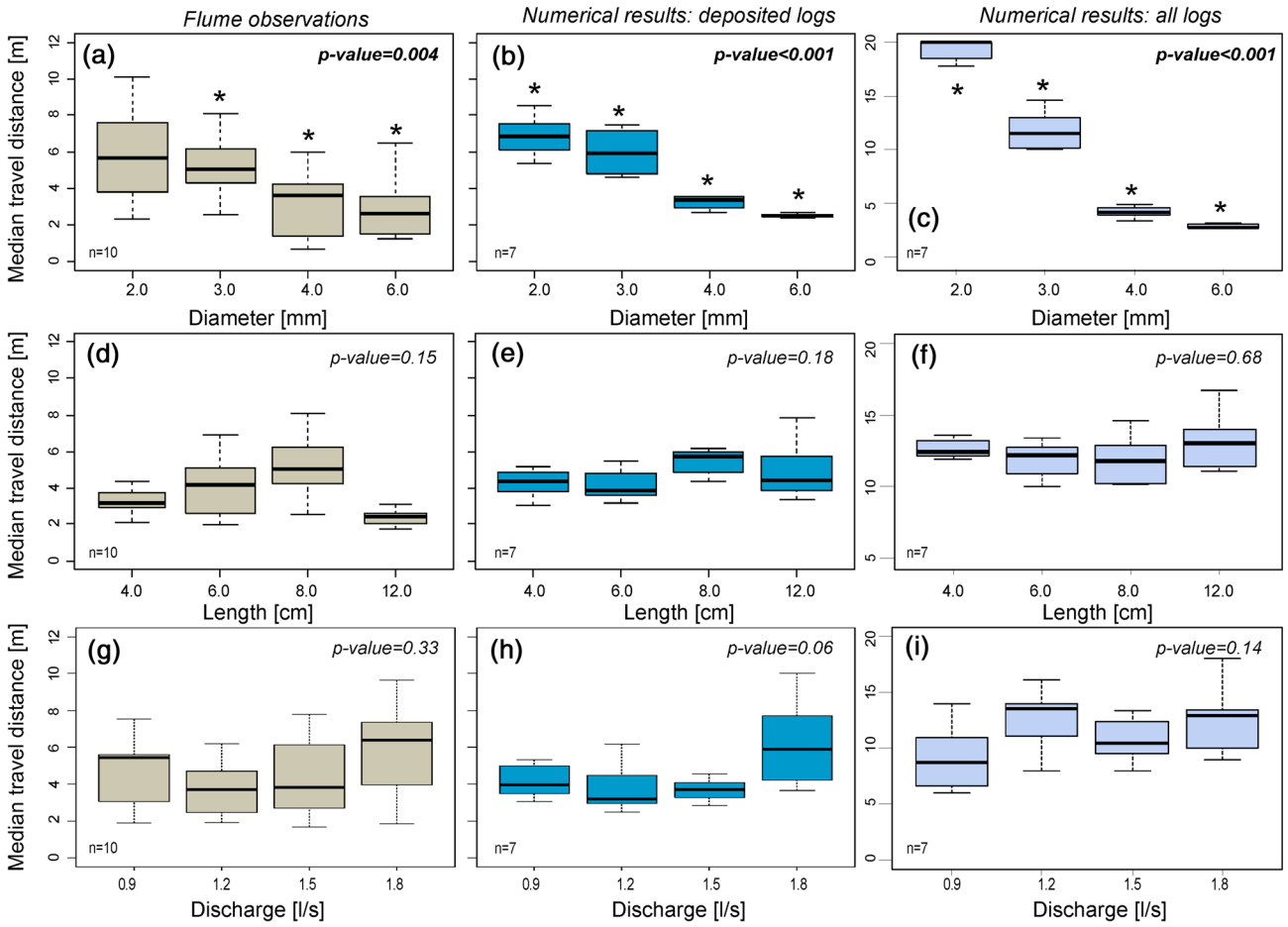

Figure 5. Ensembled results of flume observations (a-d-g) and numerical simulations (b-c-e-f-h-i) for set T1 using logs with different diameters (a–c) and different lengths (d–f); for set T2 using different discharges (g–i) and logs with the same size ($D = 3$ mm; $L = 8$ cm); n shows the sample size, here the number of runs. Boxplot values as in caption of Figure 4. The p values are from the Kruskal-Wallis test; the black stars show the groups that are significantly different according to the post hoc test.

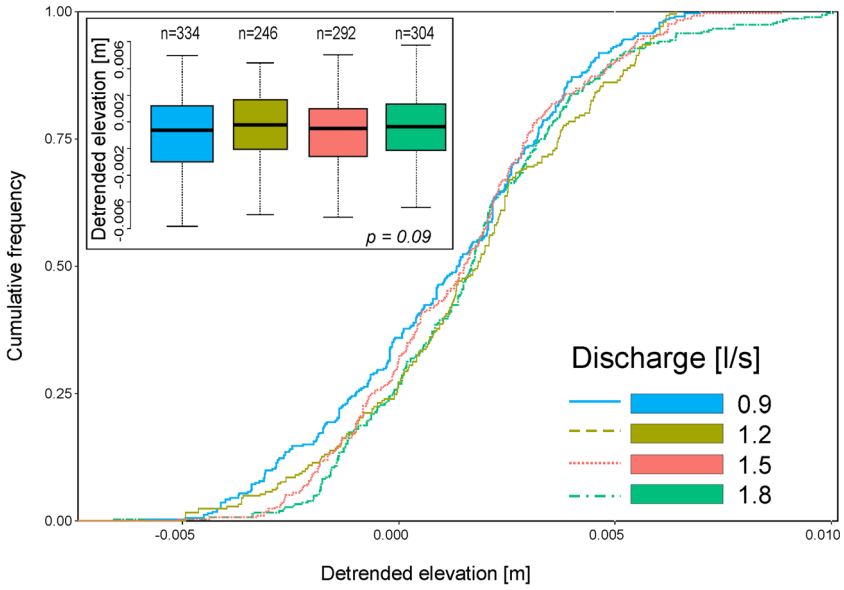

Figure 6. Cumulative distribution function of the detrended elevation of deposited logs for Set T2. The small panel shows the boxplots (*n* is the sample size, here deposited logs). The *p* values are from the Kruskal-Wallis test.

The numerical model provided accurate maps of water depth and flow velocity, which allowed us to analyze flow conditions in preferential sites for deposition. We computed the specific discharge (or discharge per unit width) as the product of flow velocity and water depth (Figure 7).

As can be seen in Figure 7, 80% of the logs were deposited in areas with specific discharge lower than 0.0005 m^2/s. This value is the result of water depth lower than 0.006 m and flow velocity lower than 0.09 m/s. According to these results, and for simulated logs with a diameter equal to 3 mm, length of 8 cm and a density of 800 kg/m^3, these were the critical flow values for deposition.

3.3. Wood Depositional Patterns and Jam Formation

We observed a strong relationship between the location of bars and wood deposits (Figure 8). The longitudinal distribution of wood deposits was conditioned by the longitudinal distribution of bars, with a significant downward trend (i.e., with larger number of logs deposited on the bars located closer to the inlet), as it was also observed in the flume. Most logs (>50%) were deposited in the most upstream part of the flume (within the first 10 m) on bars and shallow areas, whereas the number of deposited logs significantly decreased further downstream (Figure 6).

This pattern was slightly different for DEM1 and DEM3, but numerical results showed similar downward trends as observed in the flume (see maps in Figures 7 and 13 and Figure S1 in the supporting information).

The accumulation of logs in jams was also analyzed and compared with the flume experiments (Figure 9).

Figure 9 shows slightly different results comparing flume observations with numerical model results, although similar patterns were also observed. One main difference was the proportion of jams with more than nine logs, which was in general larger in the flume. Besides the absolute values, numerical model results showed that the proportion of jams with more than four logs, and even with more than three logs increased with increasing log diameter, reducing the number of single logs, as also observed in the laboratory. Logs with 4 and 6 mm diameter were prone to accumulate in jams more easily than smaller logs, forming jams with a larger number of logs, both in the flume experiments and in the simulation results. The largest logs, with diameters of 6 mm, accumulated in jams with the largest number of logs, both in numerical simulations and in the flume. The role of log length was not so evident from the numerical model results. The pattern resulting from numerical simulations was complex, as was the pattern observed for median travel distance (see next section). Shorter logs, with length of 4 cm accumulated forming jams with the lowest number of logs, both in the flume and numerical results. The proportion of large jams (accumulations with

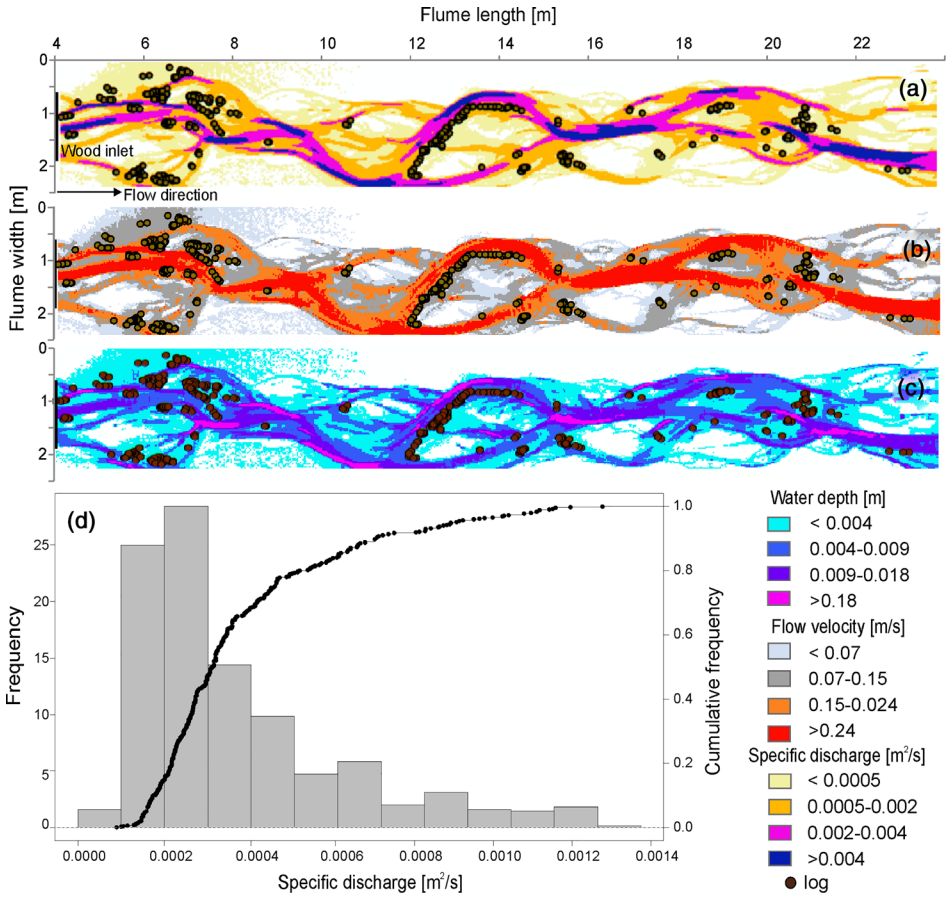

Figure 7. Map showing deposited logs (center of mass) from ensembled results from T1 and DEM1 and (a) maximum specific discharge (i.e., product of maximum water depth and maximum flow velocity for a discharge equal 1.8 l/s); (b) flow velocity; and (c) water depth. (d) Histogram and cumulative distribution function of the values of specific discharge where logs were deposited.

more than nine logs) increased for simulations with logs of 8 and 12 cm in length, as observed in the laboratory. Discharge also affected log accumulation and jam formation, with simulation results showing an upward trend in the proportion of single logs and small accumulations (jams with two logs) for increasing discharge. The lowest discharge (i.e., 0.9 l/s) enhanced the accumulation of jams with a larger number of logs (between 2 and 9). This pattern was also observed in the flume.

3.4. Sets T3 and T4: The Influence of Roots and Wood-Size Distribution

The median deposition ratio for these sets was 80% and 88%, respectively.

The presence of roots influenced the motion and deposition of wood, both in the flume and in numerical simulations (Figures 10a-10b-10c). Logs with roots were less mobile and traveled significantly shorter distances (Mann-Whitney p value < 0.005) according to the numerical model results, and as observed in the flume. Moreover, numerical model results proved that logs with roots were more likely deposited at higher elevations (Figures 10d and 10e), mostly at the top of bar surfaces, as observed during flume experiments.

The presence of roots significantly influenced the formation of log jams or wood accumulations, with an increase in the number of accumulations with more than 3 logs (Figures 10f and 10g).

Figure 11 shows the effect of log size distribution on total travel distance. We compared homogeneous distributions of logs with the same size, length and diameter with a nonhomogeneous (i.e., variable) distribution of logs of different sizes. The nonhomogeneous log size distribution significantly reduced the mobility of logs compared to homogeneous distributions with small, medium, and long logs (as reveled by the survival

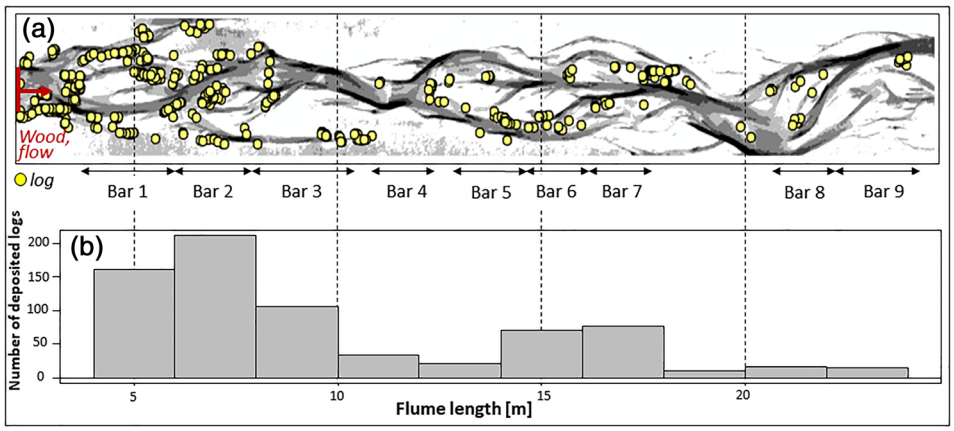

Figure 8. (a) Longitudinal distribution of the ensemble of 719 deposited logs from Set T1 and DEM2. Maps show the water depth (gray colors for values ranging between 0.005 and 0.04 m) for discharge 1.8 l/s (numerical model results) and the logs center of mass (yellow circles); (b) histogram of the number of deposited logs by longitudinal length of the flume.

curves shown in Figure 11a). The travel distance probability and median travel distance of all and only deposited logs (Figures 11b and 11c) were significantly smaller for large logs, so the presence of large logs in the nonhomogeneous distribution was key in reducing log mobility.

The size distribution influenced jam formation as well. The proportion of larger jams (greater than three logs) was larger for simulations with variable log size distribution than for small and medium sizes, but smaller when compared to large logs (see supporting information Figure S2).

3.5. Set T5: Wood Dynamics Under Unsteady Conditions

The wood supply during the hydrograph slightly influenced the transport and deposition of logs. In general, logs supplied only during the rising limb of the hydrograph traveled slightly longer distances than logs supplied under steady conditions and logs supplied with an unsteady power law along the hydrograph (Figures 12 and 13); however, differences were not statistically significant (see Figure S3 in supporting information). It is important to note that the number of supplied logs varied for each scenario. For wood supply during the rising limb with a rate of 8 and 16 logs/min, 76 and 152 logs were entering the numerical simulation, while for the unsteady supply with the power law and the steady supply along the entire hydrograph, 159 logs were modeled. In general, the larger the number of supplied logs the larger the number of deposited logs (Figure 12d), but most logs were deposited before and during the peak of the flow hydrograph (i.e., during the rising limb), with only few being remobilized and deposited during the falling limb (Figures 12a–12c). Only the case of logs supplied with an unsteady power law along the hydrograph showed a different behavior, with some logs being mobilized also during the falling limb (Figure 12c).

The number of deposited logs was larger for the unsteady wood supply using the power law (72%) than for the supply rate during the rising limb (50% and 51% of logs were deposited for supply rates of 8 and 16 logs/min, respectively), for which we observed an enhanced wood transport with a smaller number of logs deposited within the domain.

The elevation of the deposited logs did not vary significantly between the different wood supply scenarios (Figure 13), but small changes were observed during the peak of the hydrograph and the final step.

The different wood supply scenarios had a small effect on jam distribution and size. The percentage of single logs at the end of the hydrograph was slightly higher for wood supply during the rising limb (63% and 60% for supply rates of 8 and 16 logs/min, respectively) than for unsteady supply with the power law (54%). However, we observed that these values varied along the hydrograph: at the peak of the hydrograph the number of single logs for wood supply during the rising limb was 58% and 65% for rates of 8 and 16 logs/min respectively, and 71% for the unsteady wood supply. This means that during the falling limb, some jams were dismantled only in the 8 logs/min rate supply, whereas jam size increased in the other two cases.

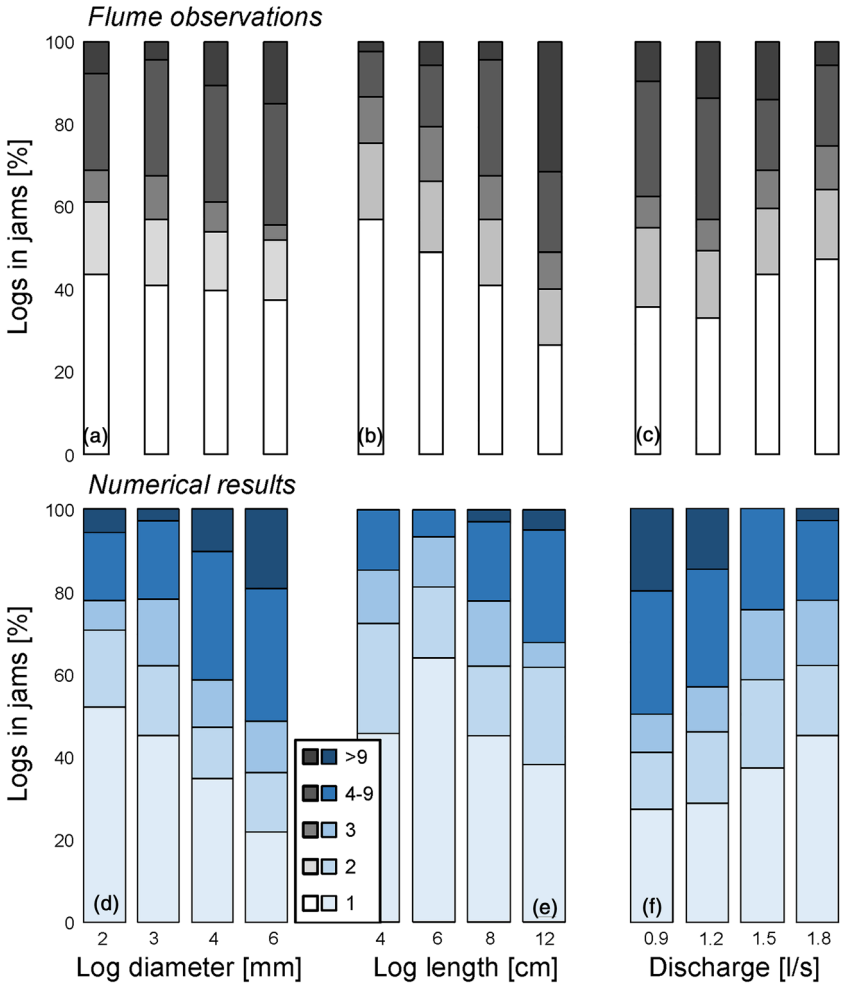

Figure 9. Percentage of deposited logs per jam (1 or single logs, jams with 2, 3, between 4 and 9, and more than 9 logs) accumulation for different values of log diameter, length and discharge (results from Sets T1 and T2) observed in the flume (a–c) and resulted from numerical simulations (d–f).

4. Discussion

This section discusses several aspects of this work. First, we discuss the challenges in calibrating numerical models, and the sensitivity of input parameters on model results. Second, we stress the important role that scaling effects may have on flume experiments and how these effects may not be fully reproduced by numerical models. Finally, we discuss the obtained results and relate them to wood dynamics in braided river morphologies at the scale of natural rivers.

4.1. Sensitivity and Calibration of Numerical Models

Numerical models have become important tools for understanding fluvial systems (Kasvi et al., 2015), as they may help to solve different environmental questions and as they allow reproducing past events and to explore scenarios. However, numerical models are simplified representations of real-world phenomena (Hardy et al., 2003), and there are often questions about the trade-off between enough field data and model reliability (Hardy et al., 2003; Rodriguez et al., 2004). Information about model capability, sensitivity to parametrization, as done in this work, and sources of uncertainty is thus essential when using numerical modeling.

Calibration of bed roughness was performed taking advantage of inundation maps observed at different discharges. This procedure has proven valuable for cases in which direct depth and velocity measurements are not available (Javernick et al., 2018), therefore providing a correct reproduction of the wet area and the bank

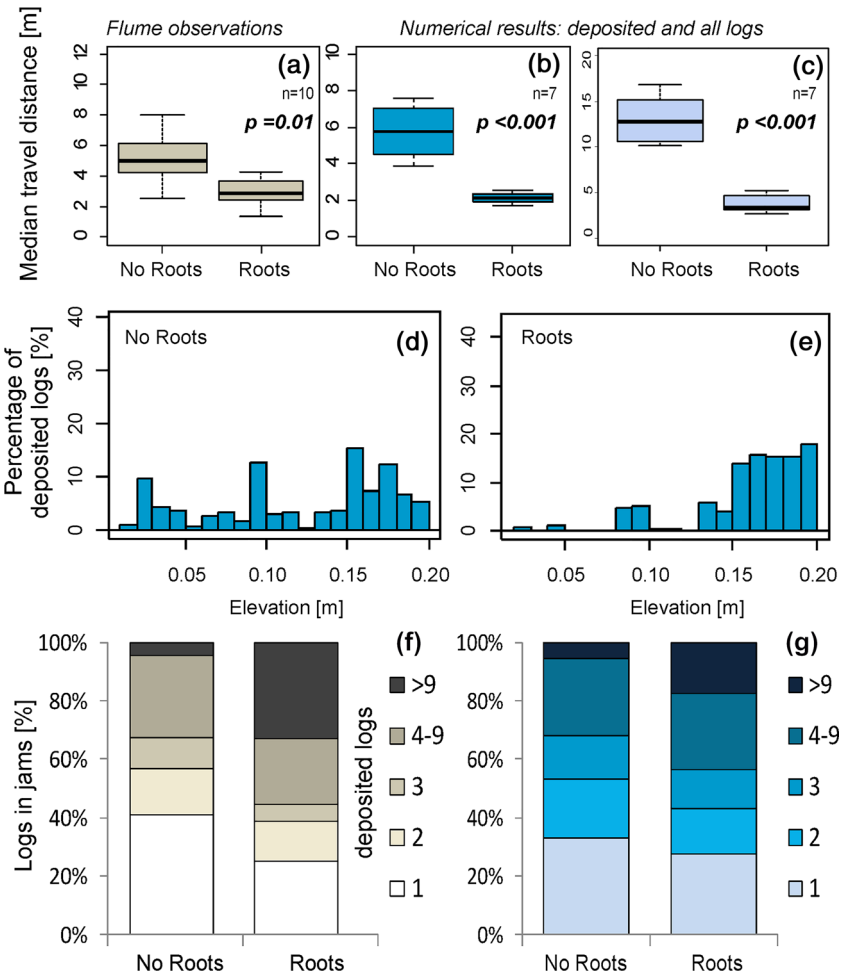

Figure 10. Ensembled flume observations (a) and numerical simulation results (B, C) for set T3 using deposited (B) and all (C) logs with and without roots; the *p* values are from the Mann-Whitney test.; (D-E) histograms of the distribution of elevation of deposited logs with and without roots; proportion of wood deposits with and without roots with single logs and accumulations of 2, 3, 4–9 and > 9 logs observed in the flume (F) and resulted from numerical simulations (G). Logs size D = 3 mm, L = 8 cm, Q = 1.8 l/s.

line. This is particularly relevant in these simulations, as the occurrence and location of shallow flows exerts key control on wood deposition.

Two way coupling of a hydrodynamic model with a wood transport model (as in Iber-Wood) introduces a set of new parameters related to the wood dynamics, which are often difficult to calibrate directly and accurately. A sensitivity analysis is therefore an ideal tool to understand the influence of input parameters on the results. For braided morphologies, characterized by generally shallow flows, the drag coefficient plays a minor role, as logs do not only float (when drag coefficients may have a stronger effect), but they mostly drag (i.e., slide and roll) on the bed, and thus, friction coefficient has a larger effect. The restitution coefficient played a small role, mainly for extremely low values. As shown here, bed topography and bank shape might be the major controls, driving log deposition. Therefore, the use of standard literature values for these coefficients (i.e., $C_d = 1.41$, $F_c = 0.47$, and $R_c = 1$) is not causing major inaccuracies, provided that the flow conditions are characterized by shallow depths and strong local variability. Values for these coefficients should be carefully selected and their impact should be explored under different conditions (e.g., floating logs in a deeper flow).

Still, differences persist between flume experiments and numerical model results. One of them was the number of logs exiting the flume domain at the outlet boundary during the laboratory experiments and those

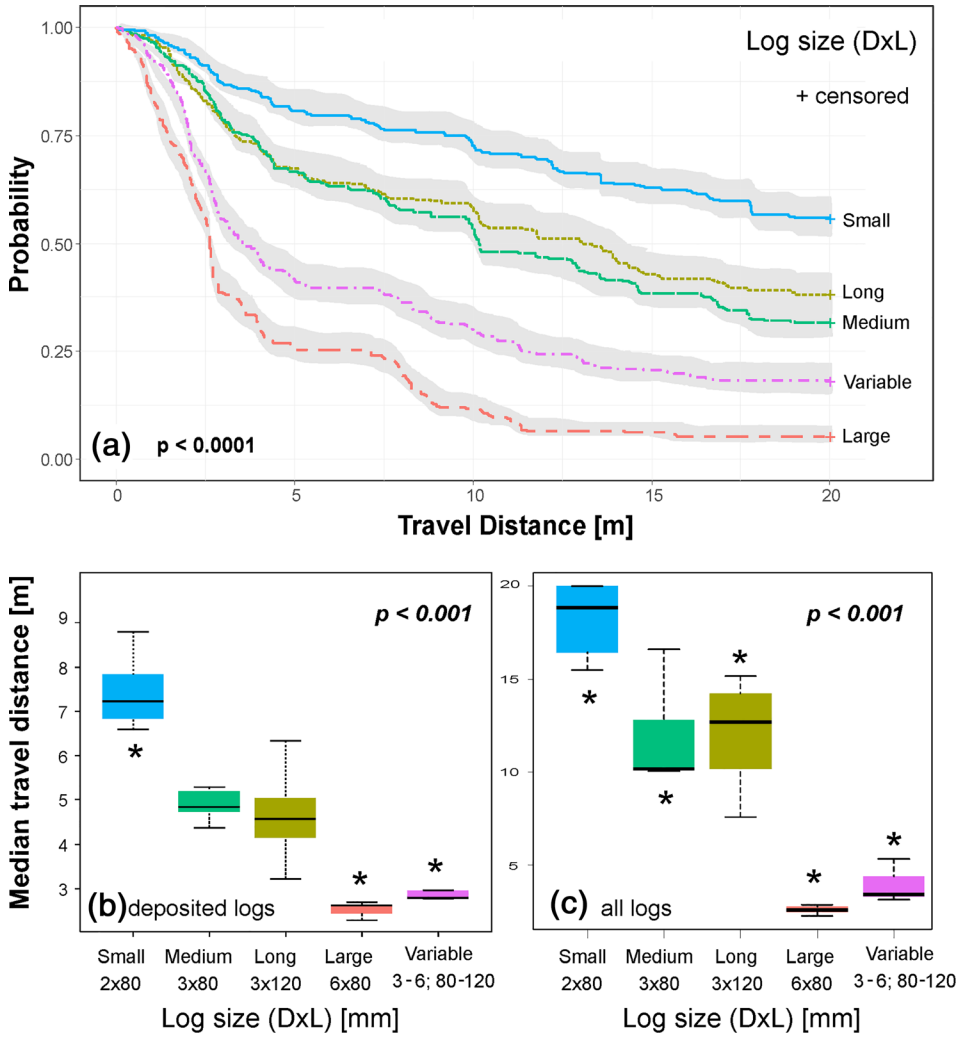

Figure 11. (a) Survival curves (i.e., probability distribution) of travel distance by all logs and boxplots of ensemble median distance of (b) deposited and (c) all logs for the different runs of Set T4 using the three DEMs and logs with different log size distributions (small, medium, long, large, and variable). Gray areas and *p* value in (a) show the confidence intervals and the log rank test results, respectively. The *p* values in (b) and (c) are from the Kruskal-Wallis test; the black stars show the group that is significantly different according to the post hoc test.

exiting the simulation domain in the numerical runs. According to the numerical simulations, the depositional ratio ranged between 42% and 97% for all sets. These values were lower than those observed in the flume (where the average depositional ratio was 98%). The lowest deposition ratios resulted from simulations using DEM1 (where Dr ranged between 42% and 89%). This discrepancy can be explained by at least three major issues. A first explanation is related to the differences in terms of the geometry used for the numerical simulations. The DEMs did not cover the full flume morphology, and some morphological features (e.g., secondary channels and bars) were not included in the DEM as compared to the flume (the DEMs were narrower and shorter than the actual flume). Second, some of the intrinsic limitations of the numerical calculations, which may not account for the real complexity of wood motion; (i) the numerical simulations did not consider sediment transport (as was considered minimal in the experiments according to Welber et al., 2013); (ii) the presence of some subsuperficial flow (i.e., flow through the gravel), that could happen in the flume with the related effect on wood motion and deposition was not modeled; (iii) the current version of the numerical model does not reproduce the secondary currents that may appear in curved channels, which may also influence the trajectory and thus the deposition of logs. Third, scaling effects that are further discussed in the following section. These

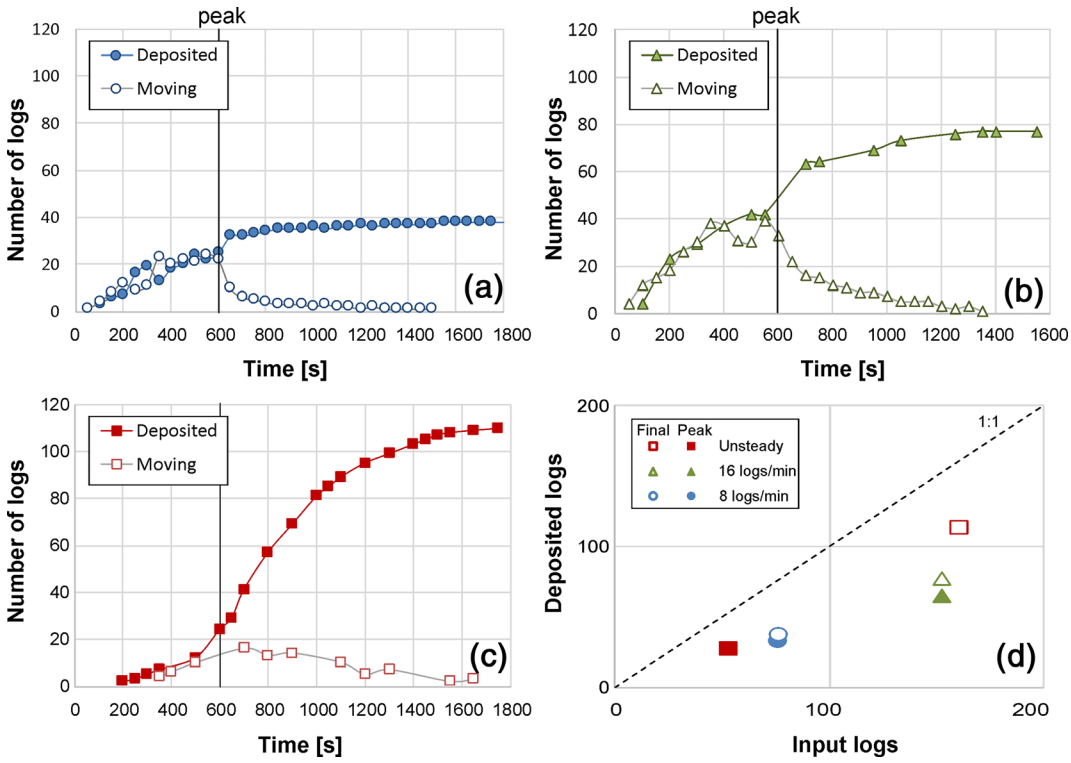

Figure 12. Number of deposited and moving logs for the different scenarios from Set T5: (a) steady rate of 8 logs/min and (b) 16 logs/min during the rising limb; (c) unsteady wood rate as a power function of the water discharge; (d) supplied and deposited logs during the three scenarios.

limitations may explain the increased number of exited logs and the overestimated travel distance in the numerical runs. Another important issue was related to the variability of travel distance between the different runs, with numerical result ensembles being smaller than the ones observed in the flume (see Figures 5 and 10). The numerical model, as a deterministic model, is not able to reproduce stochasticity of wood transport fully in complex braided morphologies as observed in the flume. In the physical model, local effects, even at the grain-size scale, may have an impact on the very shallow flows occurring in most of the wood depositional sites. In addition, and as mentioned before, the occurrence of minimal sediment

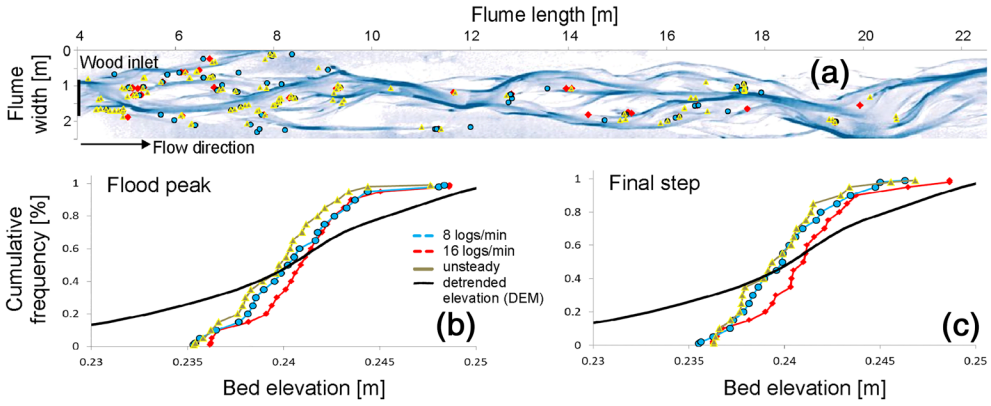

Figure 13. Longitudinal distribution of the ensemble of deposited logs from Set T5 and DEM2. Maps show the water depth (blue colors for values ranging between 0.005 and 0.04 m) for discharge 1.8 l/s (numerical model results) and the logs center of mass (red, blue, and yellow markers); (b) cumulative distribution function of deposited logs by detrended bed elevation during the peak of the hydrograph and the final step (c).

transport and the consequent reworking of bed morphology may add a further source of internal variability that cannot be captured by the numerical model. Other scaling effects are further discussed in the following section.

Furthermore, the numerical model slightly underestimates jam size. It reproduces the effect of different parameters correctly and provides good estimates of the proportion of logs deposited as single logs (see Figure 9); however, it underestimates large jam sizes as well as their occurrence. This is likely caused by the fully 3-D process of jam formation, with logs accumulating in the vertical direction (e.g., Schalko et al., 2019), which is not accurately reproduced by a 2-D model as Iber-Wood.

4.2. Scaling Effects in Small-Scale Physical Models and Effects on the Numerical Simulations

Observed differences between the physical and numerical model may also be caused by the relatively small scale of the flume experiments. Hydraulic and morphological physical models are generally scaled to refer to the Froude similarity, which guarantees correct reproduction of the ratio between inertial forces and gravity. This means that the flow field and the sediment transport processes are similar to those in the prototype when the flow is rough turbulent. However, unavoidably the Reynolds number (i.e., the effect of viscous forces) and the Weber number (i.e., the effect of surface tension; Peakall & Warburton, 1996) are different from those in the prototype. To avoid viscosity and surface tension effects, Reynolds number should be $>10^4$ (Hughes, 2005), depth should be >0.005 m and the Weber number <11 (Novak et al., 1990; Heller, 2011). In the experiments reported by Welber et al. (2013), large areas exist where these conditions were unlikely met (as verified by numerical model results; see Figure S4). In that case, wood transport and, in particular, wood deposition may be affected, as it occurs mainly in very shallow areas, often with a flow depth smaller than 0.005 m. This, on one hand, is consistent with the observed overestimation of the travel distance (and thus logs exiting the simulation domain). On the other hand, the model is probably likely to underestimate jam size, considering that in the physical model logs may stop due to surface tension, and this surface tension is not considered in the numerical calculations. This is probably not likely to significantly change the general wood deposition patterns.

4.3. Wood Dynamics in Braided Morphologies

As shown by the results presented here, in braided morphologies, wood diameter appeared to be the dominant wood property governing wood travel distance, whereas wood length exerted a comparably weaker control. These relationships between the wood size and wood transport and deposition were already shown in flume experiments (Braudrick et al., 1997; Braudrick & Grant, 2001; Welber et al., 2013) and numerical modeling (Ruiz-Villanueva, Wyzga, Zawiejska, et al., 2016). In fact, dimensionless ratios have been proposed to describe transport and deposition of wood in rivers (Braudrick & Grant, 2000, 2001), such as the relative log length, which is log length divided by channel width (L/w); and relative log diameter, which is the diameter divided by average channel depth (D/h). According to the results presented in Figure 7, the relative log diameter was 0.5. However, our results also show that the relative log diameter does not fully explain wood deposition. In fact, the presence of areas with shallow water with a sufficiently high flow velocity could also result in wood motion. Therefore, the flow conditions resulting from the discharge and the river morphology are key drivers of wood dynamics (Blauch & Jefferson, 2019). However, this relationship between discharge and braided morphology is complex. In such large rivers with multi-thread morphology, the widespread occurrence of shallow water, large exposed bars, and bank erosion would exert a strong topographical control on wood dynamics (Bertoldi et al., 2013; Gurnell et al., 2000, 2002; Le Lay et al., 2013; Ruiz-Villanueva, Piégay, Gurnell, et al., 2016). Thus, the river morphology controls wood dynamics (Ruiz-Villanueva, Wyzga, Hajdukiewicz, & Stoffel, 2016; Wyzga et al., 2015). In braided systems, an increased discharge determines a wider wet area, with a minimal increase in average water depth, shifting ideal conditions for deposition laterally more than vertically. This may explain why we did not observe significant differences in terms of elevation of deposited logs. Our observations open the door for a search of new metrics to better describe subreach characteristics that significantly impact wood transport and accumulation. An improved knowledge on where logs are more likely to be deposited by different floods provides relevant information for river and flood management and on the possibility to develop new vegetated patches and pioneer islands (Gurnell & Petts, 2006; Gurnell et al., 2018).

The presence of roots or the size distribution of supplied wood are controlling wood motion and deposition as well. Logs with roots were less mobile (both in the flume and in the numerical simulations) and traveled significantly shorter distances than logs without roots in agreement with previous studies (Abbe & Montgomery, 1996; Braudrick & Grant, 2000; Cadol & Wohl, 2010; Iroumé et al., 2018; Welber et al., 2013). According to the observations made during the flume experiments, we observe that logs with roots aligned parallel to the flow with their rootwads located upstream were, in some cases, slowly pushed downstream by the drag force exerted on the rootwad, but that the rootwad prevented logs from rolling and, therefore, limited their mobility (Welber et al., 2013).

Notably, all these variables (i.e., wood size, discharge, and distribution) influenced the formation of wood jams. According to the results shown here, larger and longer logs enhanced the formation of logjams, whereas larger discharges reduced the number of large accumulations. The increased deposition of logs with roots enhanced the accumulation of wood in jams. As observed in the flume and according to our numerical results, the presence of roots increased the frequency of large and very large jams (more than four and nine logs; see Figure 10). This effect was also comparable to that observed for the largest logs, which significantly reduced the mobility of logs and enhanced the accumulation of jams. When large pieces were included in a nonhomogeneous distribution, the distance traveled by logs was significantly reduced compared to homogeneous distributions of smaller logs. This is explained by the fact that these long pieces as well as pieces with roots act as key logs (Manners & Doyle, 2008), thereby providing nuclei for the accumulation of wood in jams (Davidson et al., 2015). In the absence of any other natural obstacles, such as living trees or big boulders, wood size and the presence of roots seem to be relevant variables controlling wood mobility and the formation of wood jams in braided rivers. Wood jams play an essential role in regulating the ecology and morphology of river systems (Scott et al., 2019), however, the formation, dynamics, and evolution of wood accumulations is still not well understood. Our results shed light into these processes.

Finally, wood in rivers is usually mobilized during floods, and thus wood dynamics should be analyzed under unsteady conditions. In this work, we designed one flood hydrograph and several wood supply scenarios and observed that in those cases where wood was supplied during the rising limb of the hydrograph, it was traveling longer distances than when supplied along the entire flood. In addition, most of the wood was deposited before the peak of the flood, with few accumulations dismantled and remobilized during the falling limb. These observations agree with those made by Schenk et al. (2014) and MacVicar and Piégay (2012), who found that most wood was mobilized at the very beginning of the floods, and by Ravazzolo et al. (2015) who observed that most of their tagged logs were deposited before the flood peak.

5. Conclusions

In this work we combined results of a laboratory physical model with a 2-D numerical model to reproduce large wood transport, deposition, and accumulation in shallow braided rivers. The combination of model results proved particularly valuable, as we took advantage of the controlled environment and similar simplifying hypothesis on wood shape (cylindrical logs with or without simplified root wads) to both improve the numerical model and to extend the experimental results. We verified that the enhanced numerical model can reproduce wood dynamics accurately and effectively, both considering log travel distance and jam size. Moreover, the numerical model was improved to better reproduce interactions between logs and riverbed and among logs. We also performed a sensitivity analysis on the main wood modeling parameters (e.g., drag, friction, and restitution coefficients), assessing their role compared to that of log size, flow field, and bed topography. The last one was demonstrated to play a major role, as the occurrence of preferential sites for deposition, such as large exposed bars, close to the wood input location may strongly reduce the travel distance.

Finally, the calibrated numerical model was used to investigate the role of variable wood piece dimensions and of unsteady discharge on wood dynamics. We explored different wood input loads and their effect on wood deposition, in terms of local bed elevation and flow field. We show that large wood distribution is likely controlled by the largest wood pieces and depends also on how wood input is distributed during the flood. Wood availability during the falling limb of the flood increases the probability to find wood pieces deposited at relatively low elevation, therefore increasing their impact on the flow field, even at low flow. The results of this study shed light to the complex relationships between floods and wood transport and deposition in braided morphologies, and our findings might be crucial for a proper river and flood management strategy.

Data Availability Statement

Data produced during the laboratory experiments was published by Welber et al., 2013. The computer software used to generate results and analyze them is freely available. The software Iber including Iber-Wood can be download online (http://www.iberaula.es; Welber, M., Bertoldi, W., Tubino, M., (2013). Wood dispersal in braided streams: Results from physical modeling. Water Resour. Res. 49, 7388–7400. https://doi.org/10.1002/2013WR014046).

Acknowledgments
This study was partially funded by the Federal Office for the Environment (FOEN) research project "WoodFlow" (15.0018.PJ/O192-3154). We appreciate insightful comments from the Editor Professor Ellen Wohl, two anonymous reviewers, and Dr. Dan Scott, who also provided helpful suggestions regarding the survival analysis.

References

Abbe, T. B., & Montgomery, D. R. (1996). Large woody debris jams, channel hydraulics and habitat formation in large rivers. *Regulated Rivers Research & Management*, *12*, 201–221.

Alonso, C. V. (2004). Transport mechanics of stream-borne logs. In S. J. Bennett, & A. Simon (Eds.), *Riparian vegetation and fluvial geomorphology* (pp. 59–69). Washington DC: American Geophysical Union Press.

Bertoldi, W., Gurnell, A. M., & Welber, M. (2013). Wood recruitment and retention: The fate of eroded trees on a braided river explored using a combination of field and remotely-sensed data sources. *Geomorphology*, 180–181, 146–155

Bertoldi, W., & Ruiz-Villanueva, V. (2017). Physical and numerical modelling of large wood and vegetation in rivers. In D. Tsutsumi & J. B. Laronne (Eds.), *Gravel-bed rivers: Processes and disasters* (pp. 729–753). John Wiley & Sons Ltd.

Bertoldi, W., Welber, M., Mao, L., Zanella, S., & Comiti, F. (2014). A flume experiment on wood storage and remobilization in braided river systems. *Earth Surface Processes and Landforms*, *39*, 804–813. https://doi.org/10.1002/esp.3537

Bewick, V., Cheek, L., & Ball, J. (2004). Statistics review 12: Survival analysis. *Critical Care*, *8*, 389–394. https://doi.org/10.1186/cc2955

Braudrick, C. A., & Grant, G. E. (2001). Transport and deposition of large woody debris in streams: A flume experiment. *Geomorphology*, *41*, 263–283. https://doi.org/10.1016/S0169-555X(01)00058-7

Bladé Castellet, E., Cea, L., & Corestein, G. (2014). Numerical modelling of river inundations. *Ingeniería del agua*, *18*, 71–82. https://doi.org/10.4995/ia.2014.3144

Blauch, G. A., & Jefferson, A. J. (2019). If a tree falls in an urban stream, does it stick around? Mobility, characteristics, and geomorphic influence of large wood in urban streams in northeastern Ohio, USA. *Geomorphology*, *337*, 1–14. https://doi.org/10.1016/j.geomorph.2019.03.033

Bocchiola, D., Rulli, M. C., & Rosso, R. (2006). Flume experiments on wood entrainment in rivers. *Advances in Water Resources*, *29*(8), 1182–1195.

Boothroyd, R. J., Hardy, R. J., Warburton, J., & Marjoribanks, T. I. (2017). Modeling complex flow structures and drag around a submerged plant of varied posture. *Water Resources Research*, *53*, 2877–2901. https://doi.org/10.1002/2016WR020186

Braudrick, C. a., & Grant, G. E. (2000). When do logs move in rivers? *Water Resources Research*, *36*, 571–583. https://doi.org/10.1029/1999WR900290

Braudrick, C. A., Grant, G. E., Ishikawa, Y., & Ikeda, H. (1997). Dynamics of wood transport in streams: A flume experiment. *Earth Surface Processes and Landforms*, *22*, 669–683. https://doi.org/10.1002/(SICI)1096-9837(199707)22:7<669::AID-ESP740>3.0.CO;2-L

Brooks, A. P., Howell, T., Abbe, T. B., & Arthington, A. H. (2006). Confronting hysteresis: Wood based river rehabilitation in highly altered riverine landscapes of south-eastern Australia. *Geomorphology*, *79*(3–4), 395–422. https://doi.org/10.1016/j.geomorph.2006.06.035

Buxton, T. H. (2010). Modeling entrainment of waterlogged large wood in stream channels. *Water Resources Research*, *46*, W10537. https://doi.org/10.1029/2009WR008041Buxton

Cadol, D., & Wohl, E. (2010). Wood retention and transport in tropical, headwater streams, La Selva Biological Station, Costa Rica. *Geomorphology*, *123*, 61–73. https://doi.org/10.1016/j.geomorph.2010.06.015

Comper, T., Lorenzo Picco, Ernest Bladé Castellet, Ruiz-Villanueva, V. (2018). Numerical modelling of large wood dynamics in the braided Piave River (Italy): The important role of roots. 5th IAHR Europe Congress — New Challenges in Hydraulic Research and Engineering, Proc. Of the 5th IAHR Europe Congress — New Challenges in Hydraulic Research and Engineering Editor(s) Aronne Armanini and Elena Nucci, https://doi.org/10.3850/978-981-11-2731-1_210-cd

Davidson, S. L., MacKenzie, L. G., & Eaton, B. C. (2015). Large wood transport and jam formation in a series of flume experiments. *Water Resources Research*, *51*, 10,065–10,077. https://doi.org/10.1002/2015WR017446

Ghaffarian Roohparvar, H. (2019). Study of driftwood dynamics in rivers for hazard assessment. *PhD Dissertation*, Institut National des Sciences Appliquées de Lyon (INSA).

Gippel, C. J., O'Neill, I. C., Finlayson, B. L., & Schnatz, I. (1996). Hydraulic guidelines for the re-introduction and management of large woody debris in lowland rivers. *Regulated Rivers: Research and Management*, *12*, 223–236. https://doi.org/10.1002/(SICI)1099-1646(199603)12:2/3<223::AID-RRR391>3.0.CO;2-#

Gurnell, A. M. (2013). Wood in fluvial systems. In J. Shroder (Ed.), *Treatise on geomorphology*, (163–188). San Diego, CA: Academic Press. https://doi.org/10.1016/B978-0-12-374739-6.00236-0

Gurnell, A., England, J., & Burgess-Gamble, L. (2018). Trees and wood: Working with natural river processes. *Water and Environment Journal*, 1–11. https://doi.org/10.1111/wej.12426

Gurnell, A., & Petts, G. (2006). Trees as riparian engineers : The Tagliamento River, Italy. *Earth Surface Processes and Landforms*, *1574*, 1558–1574. https://doi.org/10.1002/esp

Gurnell, A. M., Petts, G. E., Hannah, D. M., Smith, B. P. G., Edwards, P. J., Kollmann, J., Ward, J. V., & Tockner, K. (2000). Wood storage within the active zone of a large European gravel-bed river. *Geomorphology*, *34*, 55–72. https://doi.org/10.1016/S0169-555X(99)00131-2

Gurnell, A., Piegay, H., Swanson, F. J., & Gregory, S. V. (2002). Large wood and fluvial processes. *Freshwater Biology*, *47*(4). https://doi.org/10.1046/j.1365-2427.2002.00916.x

Hafs, A. W., Harrison, L. R., Utz, R. M., & Dunne, T. (2014). Quantifying the role of woody debris in providing bioenergetically favorable habitat for juvenile salmon. *Ecological Modelling*, *285*, 30–38. https://doi.org/10.1016/j.ecolmodel.2014.04.015

Hardy, R. J., Lane, S. N., Ferguson, R. I., & Parsons, D. R. (2003). Assessing the credibility of a series of computational fluid dynamic simulations of open channel flow. *Hydrological Processes*, *17*. https://doi.org/10.1002/hyp.1198

Heller, V. (2011). Scale effects in physical hydraulic engineering. *Journal of Hydraulic Research*, *49*, 293–306. https://doi.org/10.1080/00221686.2011.578914

Helsel, D. R. (2012). *Statistics for censored environmental data using Minitab and R*, (2nd ed.p. 343). Hoboken, New Jersey: John Wiley & Sons, Inc.

Hughes, S. A. (2005). Physical models and laboratory techniques in coastal engineering. *Advanced series on ocean engineering*, 7, Singapore: World Scientific.

Hui, E., Hu, X., C-b, J., Ma, F., & Zhu, Z. (2010). A study of drag coefficient related with vegetation based on the flume experiment. *Journal of Hydrodynamics, Series B*, *22*, 329–337. https://doi.org/10.1016/S1001-6058(09)60062-7H

Iroumé, A., Ruiz-villanueva, V., Mao, L., & Barrientos, G. (2018). Geomorphic and stream flow influences on large wood dynamics and displacement lengths in high gradient mountain streams (Chile). *Hydrological Processes*, *32*(17), 2636–2653. https://doi.org/10.1002/hyp.13157

Ishikawa, Y., Mizuyama, T., Fukuzawa, M., (1989). Generation and flow mechanisms of floating logs associated with debris flow. J.jap.Soc. Erosion ControlEng.42 (3), 4–10 (in Japanese with English abstract).

Javernick, L. A., Redolfi, M., & Bertoldi, W. (2018). Evaluation of a numerical model's ability to predict bed load transport observed in braided river experiments. *Advances in Water Resources*, *115*, 207–218. https://doi.org/10.1016/j.advwatres.2018.03.012

Kang, T., & Kimura, I. (2018). Computational modeling for large wood dynamics with root wad and anisotropic bed friction in shallow flows. *Advances in Water Resources*, *121*, 419–431. https://doi.org/10.1016/j.advwatres.2018.09.006

Kassambara, A., Kosinski, M., Biecek, P. (2019). Survminer: Drawing survival curves using "ggplot2". R package version 0.4.6. https://CRAN.R-project.org/package%3Dsurvminer

Kasvi, E., Vaaja, M., Kaartinen, H., Kukko, A., Jaakkola, A., Flener, C., et al. (2015). Sub-bend scale flow–sediment interaction of meander bends—A combined approach of field observations, close-range remote sensing and computational modelling. *Geomorphology*, *238*, 119–134. https://doi.org/10.1016/j.geomorph.2015.01.039

Le Lay, Y. F., Piégay, H., & Moulin, B. (2013). Wood entrance, deposition, transfer and effects on fluvial forms and processes: Problem statements and challenging issues. *Treatise on Geomorphology*, *12*, 20–36. https://doi.org/10.1016/B978-0-12-374739-6.00320-1

Macvicar, B., & Piégay, H. (2012). Implementation and validation of video monitoring for wood budgeting in a wandering piedmont river, the Ain River (France). *Earth Surface Processes and Landforms*, *37*, 1272–1289. https://doi.org/10.1002/esp.3240

Macvicar, B. J., Henderson, A., Comiti, F., Oberlin, C., & Pecorari, E. (2009). Quantifying the temporal dynamics of wood in large rivers: Field trials of wood surveying, dating, tracking, and monitoring techniques. *Earth Surface Processes and Landforms*, *2046*, 2031–2046. https://doi.org/10.1002/esp

Manners, R. B., & Doyle, M. W. (2008). A mechanistic model of woody debris jam evolution and its application to wood-based restoration and management. *River Research and Applications*, *1123*, 1104–1123. https://doi.org/10.1002/rra

Mazzorana, B., Hübl, J., Zischg, A., & Largiader, A. (2011). Modelling woody material transport and deposition in alpine rivers. *Natural Hazards*, *56*, 425–449. https://doi.org/10.1007/s11069-009-9492-y

Merten, E., Finlay, J., Johnson, L., Newman, R., Stefan, H., & Vondracek, B. (2010). Factors influencing wood mobilization in streams. *Water Resources Research*, *46*, W10514. https://doi.org/10.1029/2009WR008772

Novak, P., Moffat, A. I. B., Nalluri, C., & Narayanan, R. (1990). Hydraulic Structures. Unwin Hyman, London.

Paola, C., Straub, K., Mohrig, D., & Reinhardt, L. (2009). The unreasonable effectiveness of stratigraphic and geomorphic experiments. *Earth-Science Reviews*, *97*, 1–43. https://doi.org/10.1016/j.earscirev.2009.05.003

Peakall, J., & Warburton, J. (1996). Surface tension in small hydraulic river models—The significance oftheweber number. *Journal of Hydrology (New Zealand)*, *35*, 199–212. https://www.jstor.org/stable/43944772

Persi, E., Petaccia, G., & Sibilla, S. (2016). Woody debris transport modelling by a coupled DE-SW approach. *Natural Hazards*, *91*(1), 59–74. https://doi.org/10.1007/s11069-017-2891-6

Ravazzolo, D., Mao, L., Picco, L., & Lenzi, M. A. A. (2015). Tracking log displacement during floods in the Tagliamento River using RFID and GPS tracker devices. *Geomorphology*, *228*, 226–233. https;//doi.org/10.1016/j.geomorph.2014.09.012

R Core Team (2019). R: A language and environment for statistical computing. Vienna, Austria: R Foundation for Statistical Computing.

Rodriguez, J. F., Bombardelli, F. A., García, M. H., Frothingham, K. M., Rhoads, B. L., & Abad, J. D. (2004). High-resolution numerical simulation of flow through a highly sinuously river reach. *Water Resources Management*, *18*, 177–199. https://doi.org/10.1023/B:WARM.0000043137.52125.a0

Rstudio Team (2018). Rstudio: Integrated development for R. Rstudio, Inc., Boston, MA URL http://www.rstudio.com/.R Core Team (2019). R: A language and environment for statistical computing. R Foundation for Statistical Computing, Vienna, Austria. URL https://www.R-project.org/

Ruiz Villanueva, V., Bladé Castellet, E., Díez-Herrero, A., Bodoque, J. M., & Sánchez-Juny, M. (2014). Two-dimensional modelling of large wood transport during flash floods. *Earth Surface Processes and Landforms*, *39*, 438–449. https://doi.org/10.1002/esp.3456

Ruiz-Villanueva, V., Bladé, E., Sánchez-Juny, M., Marti-Cardona, B., Díez-Herrero, A., & Bodoque, J. M. (2014). Two-dimensional numerical modeling of wood transport. *Journal of Hydroinformatics*, *16*, 1077–1096. https://doi.org/10.2166/hydro.2014.026

Ruiz-Villanueva, V., Bodoque, J. M., Díez-Herrero, A., & Bladé, E. (2014). Large wood transport as significant influence on flood risk in a mountain village. *Natural Hazards*, *74*(2), 967–987. https://doi.org/10.1007/s11069-014-1222-4

Ruiz-Villanueva, V., Piégay, H., Gurnell, A. A., Marston, R. A., & Stoffel, M. (2016). Recent advances quantifying the large wood dynamics in river basins: New methods and remaining challenges. *Reviews of Geophysics*, *54*, 611–652. https://doi.org/10.1002/2015RG000514

Ruiz-Villanueva, V., Wyzga, B., Hajdukiewicz, H., & Stoffel, M. (2016). Exploring large wood retention and deposition in contrasting river morphologies linking numerical modelling and field observations. *Earth Surface Processes and Landforms*, *41*, 446–459. https://doi.org/10.1002/esp.3832

Ruiz-Villanueva, V., Wyżga, B., Mikuś, P., Hajdukiewicz, H., & Stoffel, M. (2016). The role of flood hydrograph in the remobilization of large wood in a wide mountain river. *Journal of Hydrology*, *541*. https://doi.org/10.1016/j.jhydrol.2016.02.060

Ruiz-Villanueva, V., Wyżga, B., Mikuś, P., Hajdukiewicz, M., & Stoffel, M. (2017). Large wood clogging during floods in a gravel-bed river: The Długopole bridge in the Czarny Dunajec River, Poland. *Earth Surface Processes and Landforms*, *42*(3), 516–530. https://doi.org/10.1002/esp.4091

Ruiz-Villanueva, V., Wyzga, B., Zawiejska, J., Hajdukiewicz, M., Stoffel, M., Wyżga, B., et al. (2016). Factors controlling large-wood transport in a mountain river. *Geomorphology*, *272*, 21–31. https://doi.org/10.1016/j.geomorph.2015.04.004

Schalko, I., Lageder, C., Schmocker, L., Weitbrecht, V., & Boes, R. M. (2019). Laboratory flume experiments on the formation of spanwise large wood accumulations Part II: Effect on local scour. *Water Resources Research*, *55*, 4871–4885. https://doi.org/10.1029/2019WR024789

Schenk, E. R., Moulin, B., Hupp, C. R., & Richter, J. M. (2014). Large wood budget and transport dynamics on a large river using radio telemetry. *Earth Surface Processes and Landforms*, *39*, 487–498. https://doi.org/10.1002/esp.3463

Shields, F. D., & Gippel, C. J. (1995). Prediction of effects of woody debris removal on flow resistance. *Journal of Hydraulic Engineering-Asce*, *121*(4), 341–354. https://doi.org/10.1061/(ASCE)0733-9429(1995)121:4(341)

Scott, D. N., Wohl, E., & Yochum, S. E. (2019). Wood Jam Dynamics Database and Assessment Model (WooDDAM): A framework to measure and understand wood jam characteristics and dynamics. *River Research and Applications*, *35*, 1466–1477. https://doi.org/10.1002/rra.3481

Therneau T. (2015). A package for survival analysis in S. version 2.38, <URL: https://CRAN.R-project.org/package=survival>.

Therneau, T., & Grambsch, P. M. (2000). *Modeling survival data: Extending the Cox model*. New York: Springer. ISBN 0-387-98784-3

Turowski, J. M., Badoux, A., Bunte, K., Rickli, C., Federspiel, N., & Jochner, M. (2013). The mass distribution of coarse particulate organic matter exported from an alpine headwater stream. *Earth Surface Dynamics Discussions*, *1*, 1–29. https://doi.org/10.5194/esurfd-1-1-2013

Welber, M., Bertoldi, W., & Tubino, M. (2013). Wood dispersal in braided streams: Results from physical modeling. *Water Resources Research*, *49*, 7388–7400. https://doi.org/10.1002/2013WR014046

Wohl, E. (2013). Floodplains and wood. *Earth-Science Reviews*, *123*, 194–212. https://doi.org/10.1016/j.earscirev.2013.04.009

Wohl, E. (2017). Bridging the gaps: An overview of wood across time and space in diverse rivers. *Geomorphology*, *279*, 3–26. https://doi.org/10.1016/j.geomorph.2016.04.014

Wohl, E., Kramer, N., Ruiz-Villanueva, V., Scott, D. N., Comiti, F., Gurnell, A. M., et al. (2019). The natural wood regime in rivers. *Bioscience*, *69*(4), 259–273. https://doi.org/10.1093/biosci/biz013

Wyzga, B., Zawiejska, J., Mikus, P., & Kaczka, R. J. (2015). Contrasting patterns of wood storage in mountain watercourses narrower and wider than the height of riparian trees. *Geomorphology*, *228*, 275–285. https://doi.org/10.1016/j.geomorph.2014.09.014